Computational Study of the Mechanism and the Relative Free Energies of Binding of Anticholesteremic Inhibitors to Squalene-Hopene Cyclase[†]

Fabienne Schwab,[‡] Wilfred F. van Gunsteren,[‡] and Bojan Zagrovic*[,‡,§]

Laboratory of Physical Chemistry, ETH, Swiss Federal Institute of Technology, Zürich, CH-8093, Switzerland, and Laboratory of Computational Biophysics, Mediterranean Institute for Life Sciences, 21000 Split, Croatia

Received October 15, 2007; Revised Manuscript Received January 9, 2008

ABSTRACT: The prokaryotic monotopic membrane protein squalene-hopene cyclase (SHC) is homologous to a human enzyme responsible for cholesterol formation. Using molecular dynamics in explicit water, a single monomer of SHC was simulated using the GROMOS 45A3 force field, once in complex with an inhibitor and once in an uncomplexed form. The protein exhibits significant stability on the level of secondary and tertiary structure even outside of its native membrane environment. Analysis of the fluctuations of the complexed and the uncomplexed SHC confirms the previously made suggestions for the ligand entrance channel and reveals some of its novel dynamical features that might be of functional importance. To examine the potential of computationally designing SHC ligands and study their thermodynamics of binding, the relative free energies of binding of a series of structurally similar anticholesteremic inhibitors of SHC were calculated using single-step perturbation (SSP) and thermodynamic integration (TI) techniques. While neither technique succeeds in quantitatively matching the relatively small experimental values, TI qualitatively reproduces the relative order of the experimental affinities, but SSP does not. Detailed comparisons and potential reasons for this are given.

High blood cholesterol levels greatly increase the risk of heart disease (*1*). The average person produces about 75% of blood cholesterol in his or her liver, while only about 25% is absorbed from food. Thus, most approaches to decrease the level of cholesterol in the blood aim to reduce the cholesterol biosynthesis in the liver: in other words, they aim to inhibit the enzymes that catalyze the cholesterol-producing reaction steps. The monotopic membrane protein squalene-hopene cyclase (SHC)[1] catalyzes cationic cyclization from squalene to hopene or diplopterol in *Acyclobacillus acidocaldarius* (*2–9*). It is the prokaryotic counterpart of the human triterpene cyclase 2,3-oxidosqualenecyclase (OSC) that catalyzes a key step in cholesterol biosynthesis, the reaction of 2,3-oxidosqualene to lanosterol, a precursor of cholesterol and steroid hormones (*6*). Because of its clear sequence homology to OSC, SHC is an attractive model target in attempts to find new anticholesteremic inhibitors.

The structure of SHC (Figure 1) has been determined in crystal form at 2.0 Å resolution and refined to an
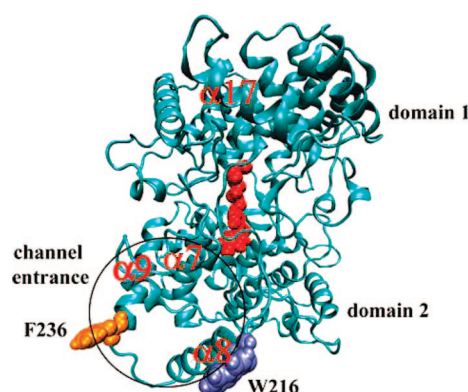

FIGURE 1: Structure of an SHC monomer. Ligand 22 bound in the binding pocket is shown in red. The putative channel entrance and the two residues that define its perimeter (F216 and W236) are highlighted.

R-factor of 15.3% (*3, 4, 10*). The pathways of the flexible educt squalene from the membrane interior to the active center cavity and of the rigid fused-ring product hopene in the reverse direction were investigated but still remain controversial. Presumably, educt access happens through a nonpolar channel that contains a narrow constriction that is still mobile enough to permit the passage of the educt in an extended conformation (Figure 1). Product release via the same channel appears to be questionable because these fused ring compounds are rigid and bulky and would require a much larger opening of the channel (*10*). In terms of its location in the cell, SHC is a monotopic membrane protein, meaning that it submerges from one side into the nonpolar part of the membrane, without fully passing through it. The protein possesses a highly lipophilic plateau around the opening of the entrance channel, where

* To whom correspondence should be addressed. Phone: 0041-44-632-5501(Switzerland); 00385-21-555-602(Croatia). E-mail: zagrovic@medils.hr, igc-sec@igc.phys.chem.ethz.ch, wfvgn@igc.phys.chem.ethz.ch.
‡ Swiss Federal Institute of Technology.
§ Mediterranean Institute for Life Sciences.

[1] Abbreviations: SHC, squalene-hopene cyclase; SSP, single-step perturbation; TI, thermodynamic integration; OSC, oxidosqualenecyclase;. rmsd, atom-positional root-mean-square difference; RMSF, root-mean-square fluctuations.

it could possibly bind to the membrane. In a model proposed to explain the binding of SHC to the membrane, the plateau region (presumably plunged into the nonpolar membrane interior) consists of two α-helices and three loops (about 15% of the protein) (*3, 7*). In its native form, SHC is a dimer, as suggested by X-ray crystallographic and gel-permeation experiments (*10*). The binding interface of the dimer lies close to the lipophilic plateau plunged into the membrane, but it is possible that dimerization is of a transient nature. Each SHC monomer consists of two structurally similar subdomains (Figure 1), possibly a result of a former gene duplication. However, the first subdomain consists of an α_6-α_6 barrel, while the second one consists of an α_5-α_5 barrel, suggesting that any potential duplication must have occurred very early. Both subdomains are stabilized through QW motifs in the outer ring. Finally, the protein contains three relevant internal cavities. The main cavity is linked to the entrance channel for the substrate at the lipophilic plateau of the protein, and it houses the substrate in the course of the reaction. Two other small cavities are located in the middle of the two α_6-α_6 barrels on opposite sides of the central cavity, and their role in the reaction is still unknown. Apart from stabilizing the structure of the enzyme, they may have no function at all (*10*).

The reaction catalyzed by SHC is a cationic cyclization cascade from squalene to hopene or diplopterol (*6*). The principal function of the enzyme is to induce the correct conformation of squalene and not to stabilize any one of the intermediate carbocations, the final base/nucleophile being a water molecule (*9*). The cyclization reaction is a highly exergonic reaction: hopene formation releases about 200 kJ/mol. This explains the requirement for the high stability of SHC, which in turn is ensured by the large number of stabilizing QW motifs present in its sequence. However, one should point out that the energy released in the reaction likely dissipates on the times scales that are much faster than any large-scale conformational changes of the protein and therefore should not play a significant role in exiting of the product.

In this study, using molecular dynamics in explicit water, a single monomer of SHC was simulated using the GROMOS 45A3 force field, (*11*) with and without an inhibitor. Despite the fact that the protein was not simulated in its native membrane environment, it exhibits pronounced stability with respect to secondary and tertiary structure. Analysis of the fluctuations of the complexed and the uncomplexed SHC gives support to the previously made suggestions for the location of the ligand entrance channel and reveals some of its novel dynamical features. In addition to gaining mechanistic insight, the main objective of the present study was to examine the potential for using computational means in designing inhibitors of SHC. With this in mind, relative free energies of binding of a series of structurally similar anticholesteremic SHC inhibitors (*8*) were calculated using single-step perturbation (SSP) and thermodynamic integration (TI) approaches. All of the inhibitors studied mimic the transition state of the cationic cyclization and contain an amine and an aromatic system, built out of two linked phenyl rings substituted with a halogen atom. While both methods reproduce certain qualitative aspects of the experimental affinities, they do not succeed in quantitatively matching the
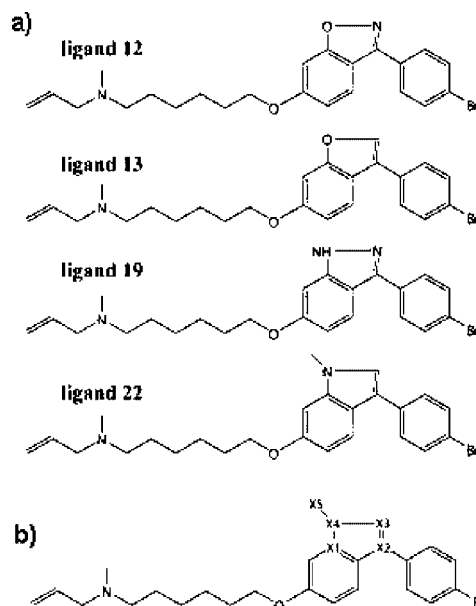

FIGURE 2: (a) Chemical structures of the anticholesteremic ligands used in the study. (b) Structure of the soft reference ligand used in single-step perturbation. Soft atoms are denoted with X.

experiment. Detailed comparison and potential reasons for this are given.

MATERIALS AND METHODS

All simulations were performed using the GROMOS05 simulation package (*12, 13*). The initial structure of SHC (620 residues) in complex with the potential anticholesteremic drug RO48-8071 was taken from the Protein Data Bank (code: 1GSZ). Two 2 ns simulations of SHC in the absence of any ligand, and two 2 ns simulations with ligand 22 (Figure 2) bound in the active site were carried out. Throughout the paper, SHC ligands are referred to according to the nomenclature in the study by Lenhart et al. (*8*) where their binding affinities were reported. For the simulations of the unliganded protein, the coordinates of the ligand were removed from the 1GSZ structure, followed by energy minimization and equilibration in a water box as described below. In case of the simulations with a ligand bound, the geometry of the ligand was derived from that of RO48-8071, followed by energy minimization and equilibration as described below.

The protein was placed in a pre-equilibrated cubic box filled with simple point charge (SPC) water molecules (*14*) (box size ∼ $10.0 \times 10.0 \times 10.0$ nm³ with 29 173 water molecules for a total of 93 911 atoms). The total charge of the protein is −15 e, but no counterions were added. To mimic the experimental conditions under which inhibitor potencies were measured (pH 6.0), His, Lys, and Arg were protonated. In all simulations, an equilibration scheme was carried out, including raising the simulation temperature from 60 to 300 K, while simultaneously decreasing the position-restraint coupling constant from 25 000 kJ/mol/nm² to 0 kJ/mol/nm² in five equidistant steps for both temperature and coupling constant. At each equilibration step, a short 20 ps simulation at constant volume was carried out. This was followed by another 20 ps at 300 K and 1 atm pressure, and a subsequent production run. Constant temperature and pressure were maintained by a Berendsen thermostat (cou-

pling time of 0.1 ps) and barostat (coupling time of 0.5 ps and isothermal compressibility of 4.575×10^{-4} (kJ/mol/nm^3)$^{-1}$), respectively (15, 16). Simulations were carried out using the GROMOS 45A3 force field, (11) using periodic boundary conditions. The atom numbers and partial charges for the newly parametrized ligands are given in the Supporting Information. A reaction-field approach was used to treat the electrostatics employing a triple-range cutoff scheme, with cutoffs of 0.8 and 1.4 nm, and a dielectric permittivity of 61 (17). The pair list was updated every five steps. The equations of motion were integrated using the leapfrog scheme and a step-size of 2 fs. Initial velocities at a given temperature were taken from a Maxwell–Boltzmann distribution. All bonds were constrained using the SHAKE algorithm (18) with a tolerance of 0.0001.

Relative free energies of binding for ligands 12, 13, 19, and 22 (Figure 2) were calculated using thermodynamic integration and single-step perturbation methods. Thermodynamic integration was implemented using the λ-coupling approach, with 21 λ-points spaced equidistantly between 0 and 1 (19). At each λ-point, the system was simulated for 500 ps, with the first 100 ps taken as equilibration and not used for calculating thermodynamic averages. To prevent instabilities, the soft-core approach (20, 21) was followed with, $\alpha_{ij}^{LJ} = 0.5$, while electrostatic interactions were treated using $\alpha_{ij}^{C} = 0.5$ nm^2. The areas underneath the $\langle \partial H/\partial \lambda \rangle$ curves were calculated using trapezoidal integration. The statistical error at each λ-point was estimated using the block averaging technique with blocks of different sizes (22).

Binding free energy differences for the above four ligands were also calculated using the single-step perturbation (SSP) technique (23–26). The free energy difference between thermodynamic states A and R can be calculated using the perturbation formula: (27)

$$\Delta G_{AR} = -k_B T \ln \langle e^{-(E_A - E_R)/k_B T} \rangle_R \quad (1)$$

where E_A and E_R denote the potential energies of the system in states A and R, respectively, k_B is the Boltzmann constant, and T is the temperature. The ensemble average (represented by the brackets) is carried out over all the configurations of state R generated in a simulation. In the SSP approach, R represents a potentially unphysical reference ligand whose configuration space exhibits significant overlap with configuration spaces of multiple different ligands of interest (24). Postanalysis of the molecular dynamics simulations of the reference ligand free in solution and bound to a receptor allows one then to calculate the relative free energy of binding between a real ligand and the reference ligand. Using eq 1 for two different ligands, one can obtain their relative free energy of binding using the following equation:

$$\Delta \Delta G_{BA} = \Delta G_{BR}(\text{bound}) - \Delta G_{BR}(\text{free}) - \Delta G_{AR}(\text{bound}) + \Delta G_{AR}(\text{free}) \quad (2)$$

The main advantage of the SSP method is that it allows one to calculate relative free energies of binding of a large series of real ligands from a pair of simulations of the reference ligand (25, 26). To facilitate sampling and make sure that the sampled configurations of the reference ligand exhibit a large-enough overlap with configuration spaces of multiple real ligands, the nonbonded interaction function of the atoms in the reference ligand is typically made soft by removing the singularity at the origin (20). In other words, the Lennard-Jones interaction involving atoms of choice is changed in such a way that there is a finite probability that two atoms fully overlap in space. This modification is applied to all those atoms that differ between different real ligands of interest.

The atoms treated as soft in our simulations are depicted with X in Figure 2. In the SSP simulations, we have tested two different softness parameters α_{ij}^{LJ} (1.8 and 2.2) for soft atoms X1 to X4, while for X5 the softness parameter was 0.2 greater (2.0 and 2.4, respectively). The reason for making X5 softer than other atoms is that only in ligand 22 this position is occupied by a methyl group, while in the other ligands it is either empty or occupied by a hydrogen atom. For the electrostatic interaction, α_{ij}^{C} was set to 0.2 nm^2 for all charged soft atoms (X1–X4). Soft atoms were assigned partial charges as follows: X1 (0.2 e), X2 (0.36 e), X3 (−0.36 e), and X4 (−0.2 e), while X5 was left neutral. The simulation of the reference ligand in water was carried out in a cubic box with sides of 3.5 nm containing a total of 1585 water molecules. The simulations of the SHC bound to the reference ligand were carried out in a cubic box with sides of ~10.0 nm containing a total of 29 173 water molecules. For both the reference ligand in water and reference ligand bound to the protein, one independent 2 ns long trajectory was run. The pre-equilibration was carried out with the real ligand as described above, followed by a 10 ps equilibration with soft parameters at constant pressure of 1 atm and subsequent production runs. Structures were saved for analysis every 5 ps for both the protein and the ligand, and every 0.2 ps for the ligand in water. Atom-positional root-mean-square differences (rmsd) were calculated after translational superposition of centers of mass and least-squares rotational fitting of atomic positions, using all or all backbone atoms of the protein, as indicated. Root-mean-square fluctuations (RMSF) around the average structure were calculated after translational superposition of centers of mass and least-squares rotational fitting of atomic positions with respect to the initial structure. Visualization of the protein and production of figures were carried out using VMD (28).

RESULTS

Two simulations initiated with different velocities, each 2 ns long, were carried out for SHC without any ligand and for SHC in complex with ligand 22 (Figure 2). The protein structure does not change significantly during any of the simulations. For both sets, the average rmsd value with respect to the starting structure equilibrates between 0.15 and 0.20 nm for backbone atoms (Figure 3) and 0.25 and 0.30 nm for all atoms (not shown). When it comes to secondary structure, more than 70% of all residues in all four trajectories remain during the entire simulation time in the identical DSSP (29) secondary structure category as in the experimental crystal structure. The flexibility of the protein was examined by analyzing root-mean-square-fluctuations (RMSF) of the protein around the average structure in the presence and in the absence of ligand 22 (Figure 4) (30). In Figure 4a we show the difference in the RMSF without and with the ligand bound: certain residues exhibit marked changes in mobility depending on whether the ligand is present or
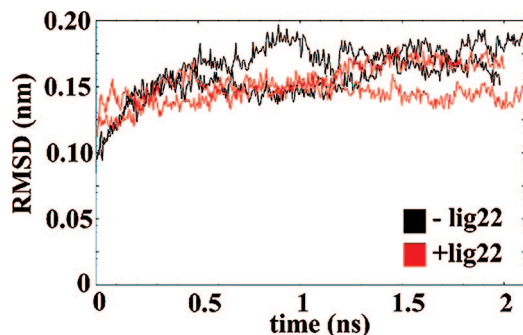
FIGURE 3: Backbone atom-positional root-mean-square difference (rmsd) from the starting structure for simulations of the uncomplexed (black) and complexed protein (red).
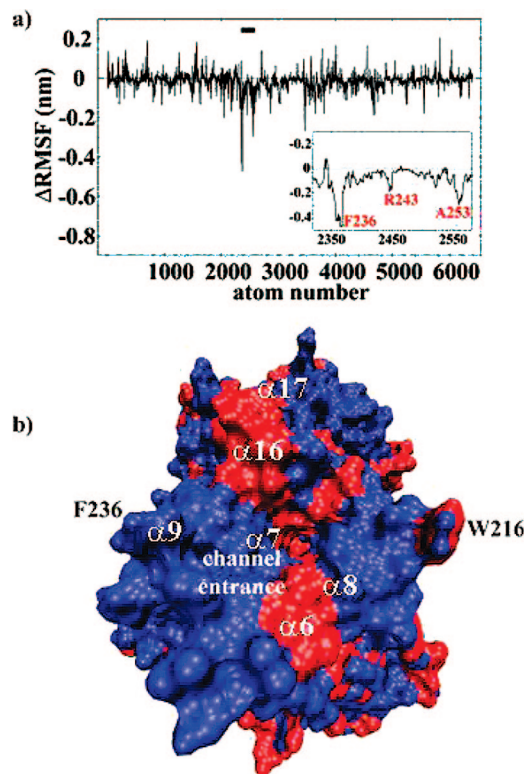

FIGURE 4: Differential atom-positional root-mean-square fluctuation (RMSF) analysis: (a) difference between the RMSF in the unliganded and the liganded state of the protein for each individual atom, RMSF(−lig) − RMSF(+lig). Region of the curve around F236 is expanded in the inset. (b) View down the entrance channel with changes in RMSF upon binding color-mapped onto the structure (atoms whose RMSF increases upon ligand binding are colored in blue and those whose RMSF decreases upon ligand binding are colored in red). Locations of the channel entrance and several pertinent α-helices are explicitly labeled.

not. In particular, helix α9, flanked by residues F236 and A253, exhibits substantial decrease in mobility when the ligand is not there. For example, the RMSF of F236 decreases by more than 0.4 nm in the absence of the ligand. What is noteworthy is that helix α9 does not directly contact the ligand. It is possible that the observed change in motion plays an important role in the gating mechanism of the enzyme, that is, substrate and product traffic. In Figure 4b we color-code the changes in the motions of the protein and their dependence on the presence of the ligand: increase in RMSF in the presence of the ligand is colored blue, while a decrease is colored red. As is apparent, complete contiguous domains of the protein undergo collective changes in motion

Table 1: Relative Free Energies of Binding[a] for the Four Ligands Studied Herein (Figure 2) from the TI Simulations and the Experiment (7)

A, B	$\Delta G_{AB}^{protein}$ (kJ mol^{-1})	ΔG_{AB}^{water} (kJ mol^{-1})	$\Delta G_{AB}^{binding}$ (kJ mol^{-1})	experiment (kJ mol^{-1})
12, 22	-9.6 ± 2.1	4.9 ± 0.6	-14.5 ± 2.7	-3.5
13, 22	-32.1 ± 2.1	-22.7 ± 0.8	-9.4 ± 2.9	-3.3
19, 22	-6.4 ± 1.4	-11.6 ± 0.7	5.2 ± 2.1	-1.2

[a] The in-water and in-protein components of the theoretical relative free energies are also given.

around the entrance channel. Notably, the linker before helix α8 (ending with W216) and the entire helix α9 increase in motion, while the linker between helices α6 and α7, the linker between helices α16 and α17, and parts of the helix α8 decrease in motion in the presence of the ligand. The potential significance of these changes in motion for substrate and product traffic in and out of the active site are further discussed below.

Because of the structural homology of SHC with the human enzyme OSC involved in cholesterol synthesis, inhibitors of SHC are generally considered to be potential anticholesteremic drugs (6, 8). To test the possibility of designing ligands for SHC and OSC, we have calculated the relative free energies of binding of four competitive inhibitors of SHC using thermodynamic integration and single-step perturbation approaches. The calculations were carried out for ligands 12, 13, 19, and 22 from Lenhart et al., (8) and the results were compared with the experimentally derived relative free energies of binding derived from the IC$_{50}$ values via

$$\Delta\Delta G_{AB}^{binding}(exp) = -RT \ln\left(\frac{IC_{50}^{A}}{IC_{50}^{B}}\right) \qquad (3)$$

Altogether, six thermodynamic integration calculations were performed, three in the protein environment perturbing the ligand 22 to ligands 12, 13, and 19, and the same three perturbations of ligand 22 in water. Comparison of the calculated relative free energies of binding with the experimental values is given in Table 1. The relative order of free energies is reproduced: $\Delta\Delta G_{12,22}^{binding} < \Delta\Delta G_{13,22}^{binding} < \Delta\Delta G_{19,22}^{binding}$. However, the $\Delta\Delta G_{19,22}^{binding}$ value obtained from the simulations is positive, and hence in disagreement with the experiment. Second, the TI results significantly disagree with the experiment on a quantitative level: relative to ligands 12 and 13, the free energy of binding of ligand 22 appears to be markedly large, while relative to ligand 19, it is too low. Overall, the root-mean-square deviation from the experimental results is 8.2 kJ mol^{-1}.

As the four ligands used in the TI calculations exhibit significant structural similarity (Figure 2), they present an ideal test case for the SSP technique. For the calculation, a total of 8 ns of simulations with the reference ligand at $\lambda = 0.5$ was carried out, twice 2 ns with a softness parameter of $\alpha_{ij}^{LJ} = 1.8$ and twice 2 ns with a softness of $\alpha_{ij}^{LJ} = 2.2$. The results are summarized in Table 2. The calculated relative free energies of binding are all negative, matching in this sense the experiment, and they are also of the same order of magnitude. However, the experimentally determined relative order is not reproduced for either setup: the ranking for the softer $\alpha_{ij}^{LJ} = 2.2$ is $\Delta\Delta G_{19,22}^{binding} < \Delta\Delta G_{12,22}^{binding} <$

Table 2: (a) Free Energy Differences between Real Ligands and the Reference Ligand for the SSP Simulations with $\alpha_{ij}^{LJ} = 1.8$. (b) Free Energy Differences between Real Ligands and the Reference Ligand for the SSP Simulations with $\alpha_{ij}^{LJ} = 2.2$. (c) Relative Free Energies of Binding for the Four Ligands Studied Herein from the SSP Simulations and the Experiment (*7*)

	(a) $\alpha_{ij}^{LJ} = 1.8$		
A	$\Delta G_{AR}^{protein}$ (kJ mol^{-1})	ΔG_{AR}^{water} (kJ mol^{-1})	$\Delta G_{AR}^{binding}$ (kJ mol^{-1})
12	−24.0	5.4	−29.4
13	−34.2	−20.7	−13.5
19	−643.7	−616.3	−27.4
22	−7.6	−1.2	−6.4

	(b) $\alpha_{ij}^{LJ} = 2.2$		
A	$\Delta G_{AR}^{protein}$ (kJ mol^{-1})	ΔG_{AR}^{water} (kJ mol^{-1})	$\Delta G_{AR}^{binding}$ (kJ mol^{-1})
12	−21.9	0.3	−22.2
13	−40.7	−26.2	−14.5
19	−643.3	−619.5	−23.8
22	−18.9	−5.4	−13.5

	(c)		
A, B	$\Delta G_{AB}^{binding}$ (kJ mol^{-1}) $\alpha_{ij}^{LJ} = 1.8$	$\Delta G_{AB}^{binding}$ (kJ mol^{-1}) $\alpha_{ij}^{LJ} = 2.2$	experiment (kJ mol^{-1})
12, 22	−23.0	−8.7	−3.5
13, 22	−7.1	−1.0	−3.3
19, 22	−21.0	−10.3	−1.2

$\Delta\Delta G_{13,22}^{binding}$, while that for the harder $\alpha_{ij}^{LJ} = 1.8$ is $\Delta\Delta G_{12,22}^{binding} < \Delta\Delta G_{19,22}^{binding} < \Delta\Delta G_{13,22}^{binding}$. What is more, the relative free energies of binding deviate in the root-mean-square sense from the experiment by 6.2 kJ mol^{-1} for the softer reference ligand and by 16.5 kJ mol^{-1} for the harder one.

DISCUSSION

Structural studies have so far not been able to adequately answer the question concerning entrance and exit channels in SHC (*4, 10*). While the identification of the entrance channel for the flexible educt squalene through the lipophilic plateau appears certain, the exit path for the product hopene seems more difficult to pinpoint. The main source of difficulty is the fact that the product hopene is a fused-ring compound and is significantly more rigid and bulky than the substrate. On the basis of the rigid model of the protein, it appears quite difficult to rationalize how the exit would occur, and it has been suggested (*4*) that a part of the energy released in the course of the cyclization reaction is utilized to significantly distort the structure of the protein for this purpose. Our simulations of apo-SHC reveal that there is a substantial change in the amplitude of the fluctuations of the outer parts of the entrance channel in the lipophilic plateau depending on whether the ligand is present or not. Certain contiguous parts of the protein surrounding the channel (most notably, the linker before helix α8, and helix α9) become markedly more mobile when a ligand is bound. One might imagine that these fluctuations could actually contribute to the exit of the rigid and bulky hopene through the same entrance channel. It is as if the scaffold of the protein is designed in such a way as to make the mouth of the channel structurally more malleable and flexible when the ligand is there. In this sense, our results are most consistent with

the scenario whereby the product exits through the entrance channel. Interestingly, while there is a noticeable change in the amplitude of the fluctuations of parts of the channel, there is very little change in their average structure. For example, in the presence of the ligand, the RMSF of F236 increases by more than 0.4 nm, while its average Cα−Cα distance to the less mobile W216 on the opposite side of the lipophilic plateau changes by less than 0.1 nm. One should also note that there is no significant change in either the fluctuations or the absolute structure of the narrowest part of the entrance channel formed by residues F166, V174, F434, and C435 that have been described as the potential gate leading to the active site. This peculiar difference in the dynamics of different parts of the channel should be further studied. Finally, the fluctuations of the QW-repeats merit comment. It has been proposed (*4*) that these motifs provide a stabilizing role and protect the enzyme against the released enthalpy of the exergonic cyclization reaction. While we have not directly simulated the reaction, our results do somewhat indirectly support this claim. Namely, the rms fluctuations of every single backbone CA atom in all eight QW-repeats in the molecule decrease in the presence of the bound ligand, indicating further tightening of the helices on the surface of the enzyme. It may be that this helps channel the dissipation of the energy released in the reaction in such a way as to prevent structural damage to the protein.

The relative free energies of binding calculated using either TI or SSP methods diverge from the experimental results. While the TI qualitatively matches the relative ordering of free energies but diverges quantitatively, the SSP results are both qualitatively and quantitatively at odds with the experiment. In the case of the TI, the discrepancy arises mainly from the perturbations in the protein. There, it appears that 400 ps sampling at certain λ-points was simply not enough to get well equilibrated $\langle \partial H/\partial\lambda \rangle$ averages, and it is possible that, with additional sampling, better agreement with experiment could be obtained.

Comparison of the SSP results reveals that the choice of the softness parameter α_{ij}^{LJ} has a considerable influence on the end result. In general, the relative free energies of binding of ligands 12, 13, and 19 with respect to ligand 22 are anywhere between 6 and 15 kJ mol^{-1} more negative for the harder SSP reference ligand compared to the softer one, and for the same reason less accurate in matching the experiment. The choice of α_{ij}^{LJ} has the biggest influence on $\Delta G_{AR}^{protein}$ of ligand 22, which is the only ligand with a methyl group at the position X5: there, the perturbation is more favorable with the softer reference ligand, presumably because of better sampling of favorable binding configurations. As the perturbations for other ligands that do not have a methyl group there are comparatively less favorable with the softer reference ligand, the net relative free energies of binding become more negative for the harder SSP reference ligand compared to the softer one. As the advantages and limitations of the SSP method are still being investigated, it appears prudent to focus more systematically on the influence of the choice of the softness parameter on the free energies that are obtained. Our results suggest that even relatively minor changes in this choice may have major impact. The better success with the softer reference ligand in our simulations suggests that perhaps the cause for the overall poor agreement

with experiment in our SSP calculations lies in inadequate sampling. While the length of the simulations may have been enough (twice 2 ns for both values of the softness parameter), the fact remains that for the calculation of the free energy differences we have saved and utilized only a total of 800 individual conformations, that is, frames for either value of the softness parameter.

One of the drawbacks of the chosen ligand series is the small range of the IC_{50} values involved. The highest IC_{50} value is 75 nM for ligand 12, the lowest IC_{50} value is 289 nM for ligand 22. This yields a maximal relative difference in free energy of binding of -3.5 kJ mol^{-1}, which is relatively small, even if there are examples of SSP studies that reached this level of accuracy (*26*). It would be interesting to use SSP to try to calculate the relative free energies of binding for all of the characterized squalene-like ligands of SHC (*7*). The largest difference in the binding free energies among those is 12.6 kJ mol^{-1}. It is likely that a better insight into the advantages and disadvantages of the SSP technique would be gained if one studied such a broader range of relative free energies of binding. The reason the four ligands studied here were chosen initially is because of their structural similarity and the possibility of successfully using a single soft reference ligand in the calculations. Because of the structural differences, studying the entire range of available SHC ligands using SSP would likely require utilizing several different soft reference ligands.

To summarize, the molecular dynamics simulation performed herein have revealed a novel and potentially functionally important dynamical picture of the entrance channel in SHC. They suggest that due to high flexibility the channel is likely to serve as an exit channel for the bulky and rigid hopene product as well. Calculations of the relative free energies of binding of four SHC inhibitors by TI and SSP suggest that further methodological improvement and/or better sampling is needed before these methods can be used to quantitatively study the thermodynamics of binding of SHC ligands and potentially design novel ones in silico.

ACKNOWLEDGMENT

SUPPORTING INFORMATION AVAILABLE

The GROMOS 45A3 computational building blocks for all the ligands studied. This material is available free of charge via the Internet at http://pubs.acs.org.

REFERENCES

1. Harvard School of Public Health. Fats and Cholesterol, 2006. http://www.hsph.harvard.edu/nutritionsource/fats.html.
2. Seckler, B., and Poralla, K. (1986) Characterization and partial purification of squalene-hopene cyclase from bacillus Acidocaldarius. *Biochim. Biophys. Acta 881*, 356–363.
3. Wendt, K. U., Feil, C., Lenhart, A., Poralla, K., and Schulz, G. E. (1997) Crystallization and preliminary X-ray crystallographic analysis of squalene-hopene cyclase from *Alicyclobacillus acidocaldarius. Protein Sci. 6*, 722–724.
4. Wendt, K. U., Poralla, K., and Schulz, G. E. (1997) Structure and function of a squalene cyclase. *Science 277*, 1811–1815.
5. Wendt, K. U., and Schulz, G. E. (1998) Isoprenoid biosynthesis: manifold chemistry catalyzed by similar enzymes. *Structure 6*, 127–133.
6. Wendt, K. U., Schulz, G. E., Corey, E. J., and Liu, D. R. (2000) Enzyme mechanisms for polycyclic triterpene formation. *Angew. Chem., Int. Ed. Engl. 39*, 2812–2833.
7. Lenhart, A., Weihofen, W. A., Pleschke, A. E. W., and Schulz, G. E. (2002) Crystal structure of a squalene cyclase in complex with the potential anticholesteremic drug Ro48–8071. *Chem. Biol. 9*, 639–645.
8. Lenhart, A., Reinert, D. J., Aebi, J. D., Dehmlow, H., Morand, O. H., and Schulz, G. E. (2003) Binding structures and potencies of oxidosqualene cyclase inhibitors with the homologous squalene-hopene cyclase. *J. Med. Chem. 46*, 2083–2092.
9. Reinert, D. J., Balliano, G., and Shulz, G. E. (2004) Conversion of squalene to the pantacarbocyclic hopene. *Chem. Biol. 11*, 121–126.
10. Wendt, K. U., Lenhart, A., and Schulz, G. E. (1999) The structure of the membrane protein squalene-hopene cyclase at 2.0 Å resolution. *J. Mol. Biol. 286*, 175–187.
11. Schuler, L. D., Daura, X., and van Gunsteren, W. F. (2001) An improved GROMOS96 force field for aliphatic hydrocarbons in the condensed phase. *J. Comput. Chem. 22*, 1205–1218.
12. Christen, M., Hünenberger, P. H., Bakowies, D., Baron, R., Bürgi, R., Geerke, D. P., Heinz, T. N., Kastenholz, M. A., Kräutler, V., Oostenbrink, C., Peter, C., Trzesniak, D., and van Gunsteren, W. F. (2005) The GROMOS software for biomolecular simulation: GROMOS05. *J. Comput. Chem. 26*, 1719–1751.
13. van Gunsteren, W. F., Bakowies, D., Baron, R., Chandrasekhar, I., Christen, M., Daura, X., Gee, P., Geerke, D. P., Glättli, A., Hünenberger, P. H., Kastenholz, M. A., Oostebrink, C., Schenk, M., Trzesniak, D., van der Vegt, N. F., and Yu, H. B. (2006) Biomolecular modeling: Goals problems, perspectives. *Angew. Chem., Int. Ed. 45*, 4064–4092.
14. Berendsen, H. J.; Postma, J. P.; van Gunsteren, W. F.; Hermans, J. (1981) In Intermolecular Forces, pp 331–342, Reidel, Dordrecht.
15. Berendsen, H. J. C., Postma, J. P., van Gunsteren, W. F., DiNola, A., and Haak, J. R. (1984) Molecular dynamics with coupling to an external bath. *J. Chem. Phys. 81*, 3684–3690.
16. van Gunsteren, W. F.; Billeter, S. R.; Eising, A. A.; Hünenberger, P. H.; Krüger, P.; Mark, A. E.; Scott, W. R. P.; Tironi, I. G. *Biomolecular Simulation: The GROMOS96 Manual and User Guide*, Biomos, Zurich, Groningen 1996.
17. Heinz, T. N., van Gunsteren, W. F., and Hünenberger, P. H. (2001) Comparison of four methods to compute the dielectric permittivity of liquids from molecular dynamics simulations. *J. Chem. Phys. 115*, 1125–1136.
18. Ryckaert, J. P., Ciccotti, G., and Berendsen, H. J. C. (1977) Numerical integration of Cartesian equations of motion of a system with constraints - molecular dynamics of *n*-alkanes. *J. Comp. Phys. 23*, 327–341.
19. van Gunsteren, W. F.; Beutler, T. C.; Fraternali, F.; King, P. M.; Mark, A. E.; Smith, P. E. (1993) In *Computer Simulation of Biomolecular Systems, Theoretical and Experimental Applications*, pp 315–348, ESCOM Science Publishers, Leiden.
20. Beutler, T. C., Mark, A. E., van Schaik, R. C., Gerber, P. R., and van Gunsteren, W. F. (1994) Avoiding singularities and numerical instabilities in free energy calculations based on molecular simulations. *Chem. Phys. Lett. 222*, 529–539.
21. Zacharias, M., Straatsma, T. P., and McCammon, J. A. (1994) Separation-shifted scaling, a new scaling method for Lennard-Jones interactions in thermodynamic integration. *J. Chem. Phys. 100*, 9025–9031.
22. Allen, M. P.; Tildesley, D. J. (1989) *Computer Simulations of Liquids*, Oxford University Press Inc., New York.
23. Liu, H., Mark, A. E., and van Gunsteren, W. F. (1996) Estimating the relative free energy of different molecular states with respect to a single reference state. *J. Phys. Chem. 100*, 9485–9494.
24. Pitera, J. W., and van Gunsteren, W. F. (2001) One-step perturbation methods for solvation free energies of polar solutes. *J. Phys. Chem. B 105*, 11264–11274.
25. Oostenbrink, C., and van Gunsteren, W. F. (2003) Single-step perturbations to calculate free energy differences from unphysical reference states: limits on size, flexibility, and character. *J. Comput. Chem. 24*, 1730–1739.

26. Oostenbrink, C., and van Gunsteren, W. F. (2004) Free energies of binding of polychlorinated biphenyls to the estrogen receptor from a single simulation. *Proteins: Struct., Funct. Bioinformatics 54*, 237–246.

27. Zwanzig, R. W. (1954) High-temperature equation of state by a perturbation method. I. Nonpolar gases. *J. Chem. Phys. 22*, 1420–1426.

28. Humphrey, W., Dalke, A., and Schulten, K. (1996) VMD: Visual molecular dynamics. *J. Mol. Graphics 14*, 33–38.

29. Kabsch, W., and Sander, C. (1983) Dictionary of protein secondary structure - pattern-recognition of hydrogen-bonded and geometrical features. *Biopolymers 22*, 2577–2637.

30. Zagrovic, B., and van Gunsteren, W. F. (2007) Computational analysis of the mechanism and thermodynamics of inhibition of phosphodiesterase 5 Å by synthetic ligands. *J. Chem. Theory Comp. 3*, 301–311.